Y. Ueda*, T. Nakajima, T. Ishii, R. Tsujino and M. Iguchi

Numerical Simulation of Gas-Liquid Two-Phase Flow in a Horizontally Placed Hydrophobic Rectangular Channel (Part 1, Influence of Abrupt Expansion)

Abstract: This paper aims to computationally investigate flow patterns of gas-liquid two-phase with an abrupt expansion. To do so, the present computation is nicely verified against the previous experimental results for a good wettability surface. These rectangular channels have a thickness narrower than the Laplace constant of the present situation. Under a poor wettability condition, this narrow thickness affects the flow pattern; e.g., the air phase forms channeling behind the expansion in a low airflow rate whereas the air phase becomes fragments of bubbles due to the expansion under a good wettability condition.

Keywords: two-phase flow, rectangular channel, wettability, abrupt expansion, CFD

PACS® (2010). 47.15.-x, 47.55.-t, 68.08.Bc

***Corresponding author: Y. Ueda:** Division of Materials Science and Engineering, Graduate School of Engineering, Hokkaido University, Nishi 8, Kita 13, Kita-Ku, Sapporo, Hokkaido 060–8628, Japan
E-mail: y-ueda@eng.hokudai.ac.jp
T. Nakajima: Division of Mechanical Engineering, Graduate School of Engineering, Osaka Prefecture University, 1–1, Gakuen-Cho, Sakai, Osaka 599–8531, Japan
T. Ishii: JFE Steel Corporation, 1–1 Minami-Watarida-Cho, Kawasaki-Ku, Kawasaki, Kanagawa 210–0855, Japan
R. Tsujino: Department of Mechanical Engineering, Setsunan University, 17–8, Ikedanaka-Machi, Neyagawa, Osaka 572–8508, Japan
M. Iguchi: Division of Materials Science and Engineering, Graduate School of Engineering, Hokkaido University, Nishi 8, Kita 13, Kita-Ku, Sapporo, Hokkaido 060–8628, Japan

I Introduction

Two-phase flow in a channel is of fundamental importance for many industrial applications such as nuclear energy plant, steelmaking plant, and oil and gas factories. In these applications, the two-phase flow occurs in complicated piping geometries that include abrupt changes of cross-sectional area, orifices, bends and valves under various flow conditions. To design such two-phase flow systems, we need to investigate flow characteristics due to the effect of these elements. In particular, this study targets an abrupt expansion among these elements.

For a two-phase flow of gas and liquid in a circular pipe, the liquid and gas phases distribute themselves into several recognizable flow structures. These are referred to as flow patterns and their majority patterns are depicted in Fig. 1, e.g., for a vertical pipe:

- *Bubbly flow*: The liquid phase is continuous and bubbles are dispersed in the liquid phase.
- *Slug flow*: Bullet-shape bubbles are formed in a pipe. Classically, Taylor [1] and Davies & Taylor [2] carried out their experiment with theoretical consideration about a shape of a slug bubble moving in a circular pipe.
- *Annular flow*: The liquid flows along the wall of a pipe as a film, and the gas phase flows in the inner region of the pipe.

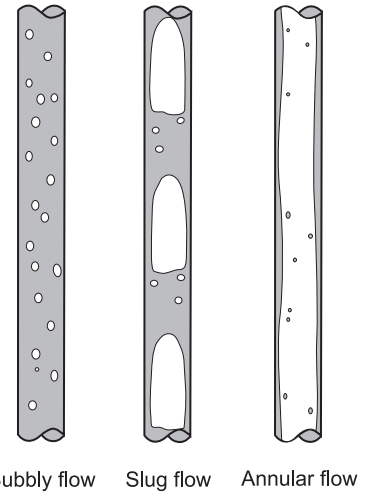

Fig. 1: Rough sketch of typical flow patterns in a vertical pipe.

To properly evaluate the local flow regime in a pipe, flow pattern maps have been made for vertical and horizontal settings (e.g., Hewitt & Roberts [3] for a vertical pipe; Baker [4] and Taitel & Dukler [5] for a horizontal pipe). At present, these flow pattern maps are advanced for various two-phase flow situations (e.g., [6–8] for a horizontal pipe; [9] for a non-Newtonian liquid). One can refer to some published textbooks, e.g., [10, 11].

The friction loss of a pipe flow can be a key quantitative data, but not easy to obtain, for designing the above-mentioned practical two-phase flow systems. The pipe friction loss can be successfully estimated using the classical parameter of Lockhart & Martinelli [12] and its simple form of Chisholm [13] which adjust the friction loss for a single-phase flow to a relevant two-phase flow.

Compared to a circular pipe flow, a rectangular duct has been scarcely dealt with the experiment. At most, a few relevant works seem to be recently published as the references [14–20]. In an extremely narrow duct, the duct height (not a hydraulic diameter) would be compared to the Laplace constant, $\sqrt{\sigma/[g(\rho_L-\rho_G)]}$, that the surface tension governs the fluid system rather than the inertia force. Here, ρ_L and ρ_G are the densities of liquid and gas, σ the surface tension, g the acceleration due to gravity. For instance, in the two-phase flow system of air and water, the Laplace constant is calculated as about 2.7 mm. Such a thin channel is known to enhance heat exchange in operation of systems that include gas-liquid two-phase flow.

The surface wettability affects the two-phase flow pattern. Indeed, Iguchi & Terauchi [21] showed that the pattern of the bubbly and slug flows changed in a vertical pipe coated with a water-repellent material, Furthermore, the effect of the wettability affects the slug movement in an inclined pipe [22].

As mentioned above, this study computationally investigates the two-phase flow in a rectangular duct of 2 mm thickness with the abrupt expansion. To evaluate the accuracy of the computation, the results of the previous associated experiment [23] are cited for a good wettability condition. Furthermore, this study selects two wettability conditions (good and poor wettabilities) on the channel surface for investigating the influence of the wettability.

II Computational procedure

The FLUENT numerical code ver. 6.2.16, a commercially available CFD software package, was employed for all numerical predictions on Intel Core 2 Quad 2.66 GHz processor with 3.25 GB RAM. GAMBIT 2.2.30 was employed for the establishment of the three-dimensional computational grid.

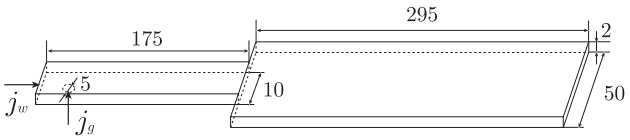

Fig. 2: Physical setup of the horizontally placed rectangular channel (units in mm).

The computational grids were made up of structured elements and a total of 132,440 cells were employed for a given flow domain in the millimeter-scale rectangular channel with the thickness of 2 mm which is shown in Fig. 2. The superficial velocities of water (denoted by j_w) and air (denoted by j_g) were given at the left side surface having $10W \times 2H$ mm (W and H indicate the width and height of the channel, respectively) and at the circular hole nozzle having $\phi 5$ mm diameter on the bottom surface, respectively (see Fig. 2). The origin of the coordinate system is set at the center of the inlet nozzle and the x-axis is taken in the stream direction. The mixed two-phase flow injected from the inlets passes through the section of the abrupt expansion and ends up outflowing from the computational domain. At the right side surface the total pressure was enforced to converge to the gauge pressure. In the present computation, three sets of superfacial velocities were selected against two values of the equilibrium contact angle θ_c as shown in Table I. The wettability is usually called *poor* for $\theta_c \geq 90°$ whereas called *good* for $\theta_c < 90°$.

FLUENT uses a control-volume-based technique to solve the governing continuity and momentum equations. A segregated implicit solver and second-order upwind interpolation scheme were employed for each computational iteration. A time-step size of $\Delta t = 1.0 \times 10^{-4}$ s was adopted to achieve a convergence in every time step. Free surface behaviour, between the water and air phases, was captured by the Volume-of-Fluid (VOF) model (Geo-Reconstruct). The tracking of the interface between the phases was accomplished by the solution of a continuity equation for the volume fraction of a phase. The surface tension of 0.0727 (N/m) was adopted. The contribution

	θ_c = 30°		θ_c = 147°
j_g = 20 cm/s, j_w = 28 cm/s	case (I)		case (III)
j_g = 80 cm/s, j_w = 10 cm/s	case (II)		case (IV)
j_g = 0.0 cm/s, j_w = 28 cm/s		case (V)	

Table I: Computational parameters.

of a volume force from a wall adhesion was added to the momentum equation as the source term, i.e., $F_{\mathrm{vol}} = \sigma_{ij}[\rho\kappa_i \nabla\alpha_i]/[(1/2)(\rho_i + \rho_j)]$ with the curvature $\kappa = \nabla \cdot \boldsymbol{n}$ and the surface normal $\boldsymbol{n} = \nabla\alpha$. Here, ρ_i was the density of the liquid i and σ_{ij} the surface tension coefficient. The wettability was taken into account using the geometrical condition $\boldsymbol{n} = \boldsymbol{n}_w \cos\theta_c + \boldsymbol{t}_w \sin\theta_c$ on the contact line where $\boldsymbol{n}_w$ and $\boldsymbol{t}_w$ were the normal and tangential vectors on a wall. In this computation, we adopted the sufficiently small time-step Δt during the bubble deformation. This allowed us to employ the following Laplace–Young equation: $\Delta p = \sigma_{12}(\kappa_1 + \kappa_2)$, where Δp is the pressure difference between the two fluids. The convergence of the computational solution was determined based on residuals for the continuity and x-, y-, z-velocities. The residual of all quantities was set to 10^{-4}. The solution was considered to be converged when all of the residuals were less than or equal to these default settings (see FLUENT 6.2 User's Guide [24] for more details).

III Results

A For good wettability (θ_c = 30°)

Figure 3 shows a comparison of the flow patterns for two sets of the superficial velocities (i.e., cases (I) and (II)) between the present computation and the previous experimental photographs [23]. Note that the flow direction is taken to be inverse in the experiment. The present computation seems to give similar flow patterns against the experimental photographs around the section of the abrupt expansion. In downstream far from the expansion, the present computed results would immediately recover a pressure drop caused by the expansion, because the outflow condition is enforced on the outlet surface of $50W \times 2H$ mm (see Fig. 2) whilst the working fluids outflow through the outlet nozzle of ϕ5 mm diameter in the experiment [23]. Therefore, in the computed result of Fig. 3 (a), the bubble fragments structure due to the expansion ends up growing to the slug flow in downstream region unlike the experimental result of Fig. 3 (b). The relationship between the flow pattern and the pressure field caused by the expansion is discussed below.

The pressure drop at the expansion is a key quantity to affect the flow pattern. To discuss this, the single phase flow with the same j_w as case (I) and zero j_g is computed as case (V). Figure 4 shows the pressure p and pressure drop $-\mathrm{d}p/\mathrm{d}x$ of case (V) on the centerline of the channel. As observed in Fig. 4, the pressure drop increases with x in the upstream duct and approaches the fully developed flow whose pressure is 830 Pa/m. The pressure drop suddenly increases at the expansion and then decreases rapidly. In particular, the pressure drop becomes weaker in downstream of $x \gtrsim 200$ mm than that in the upstream of the expansion, i.e., the effect of the expansion affects the region of $x \lesssim 200$ mm from the expansion and the memory ends up being lost in the downstream. Therefore, the fragments of the bubble due to the expansion stagnate around $x \lesssim 200$ mm from the expansion, and in a further downstream ($x \gtrsim 200$ mm) the bubble fragments recover to the original nature, i.e., slug flow (see Fig. 3 (a)). Indeed, Kumagai & Iguchi [25] showed that the situation of case (I) exhibits the slug flow in the same rectangular channel without the expansion.

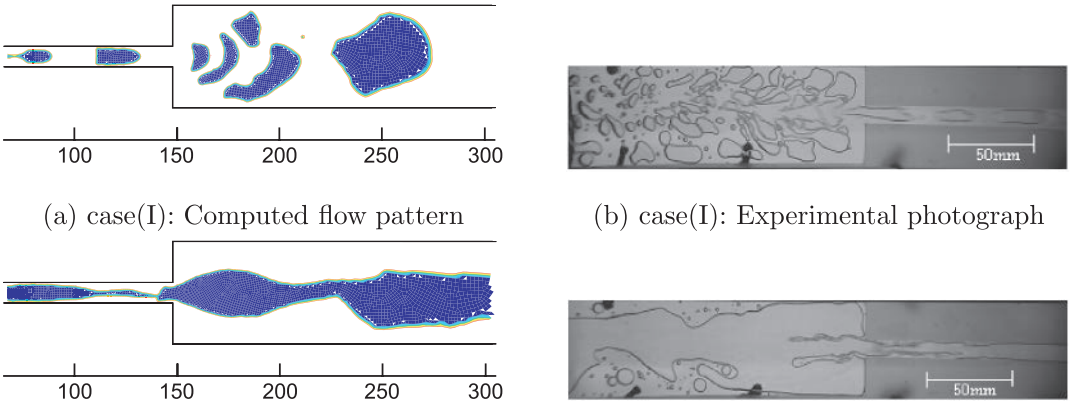

(a) case(I): Computed flow pattern

(b) case(I): Experimental photograph

(c) case(II): Computed flow pattern

(d) case(II): Experimental photograph

Fig. 3: Comparison of flow patterns for cases (I) and (II) between the present computation (air phase colored) and the previous experimental photographs [23]. Note that the stream direction is inverse between the computation and experiment.

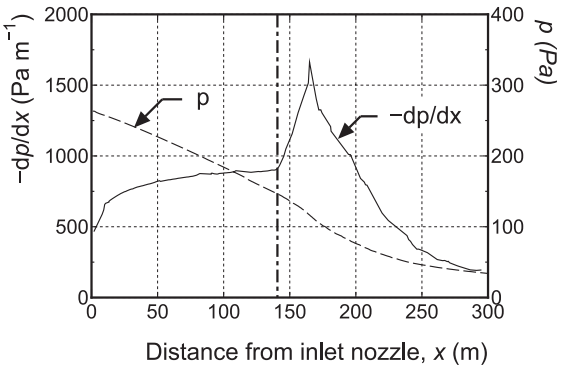

Fig. 4: Pressure p and pressure drop $-dp/dx$ on the centerline of the channel for a single-phase flow (case (V)). The abrupt expansion is located at the dot-dashed line.

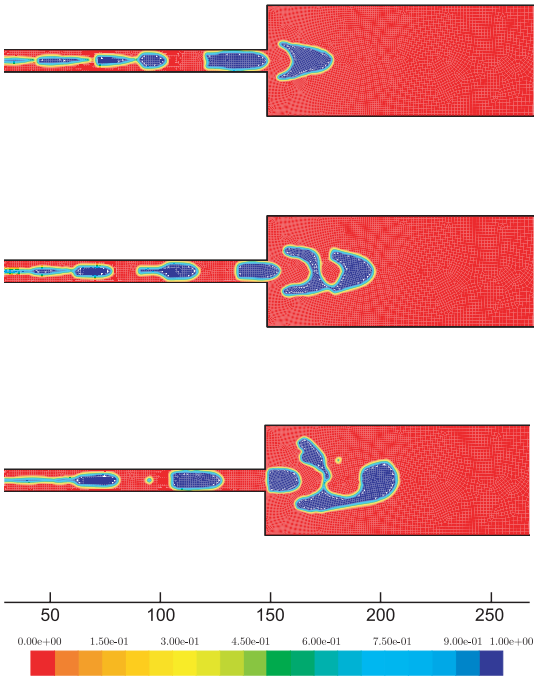

Fig. 5: Selected snapshots of bubble deformation (void fraction) at the expansion for case (I) at (top): $t = 0.4$ s, (middle): $t = 0.5$ s and (bottom): $t = 0.6$ s.

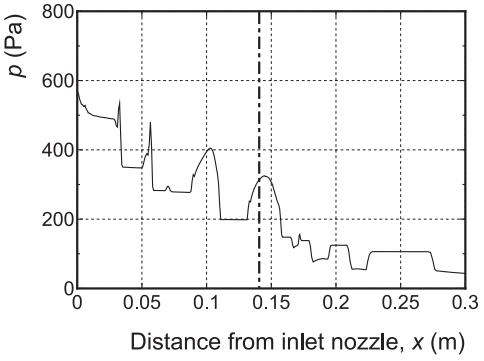

Fig. 6: Pressure p on the centerline of the channel for case (I). The abrupt expansion is located at the dot-dashed line.

As mentioned in the introduction, the pipe friction loss of the two-phase flow can be estimated using the Lockhart & Martinelli [12] parameter and its simple form of Chisholm [13] on the basis of a single-phase flow. In contrast, two-phase flow models of pressure recovery across an abrupt expansion are listed in Table 1 of Ahmed *et al.* [26] together with their revised model. To use these models on the present results, the time-averaged void fraction $\overline{\alpha}$ is needed, and unfortunately the quantity is not calculated here. This study mainly addresses computational flow patterns caused by the abrupt expansion in a narrow rectangular channel, and the quantitative discussion about the pressure drop is required for a future study.

Figure 5 shows the contour of the void fraction at the first bubble passing through the expansion. Note that the void fraction $\alpha = 0$ indicates the water phase and $\alpha = 1$ the air phase. The slug bubbles successively pass through the expansion and the bubbles are broken into fragments due to the pressure drop across the expansion. As mentioned in Fig. 4, the effect of the pressure drop due to the expansion recovers around $x = 200$ mm so that, although the bubble fragments stagnate within $x \lessapprox 200$ mm, these fragments can merge behind $x \approx 200$ mm and grow to the slug bubble (see Fig. 3 (a)). For reference, the pressure distribution of Fig. 3 (a) on the centerline is displayed in Fig. 6. The pressure seems to fluctuate due to the air phase of moving bubbles.

Under a high airflow rate condition (i.e., case (II)), the flow pattern ahead of the expansion is observed to exhibit the annular (see Fig. 3 (c)). Therefore, this airflow behaves like a jet injected from a nozzle downstream of the expansion, and the flow pattern also forms the annular in downstream of the expansion. Indeed, the experimental results of Kumagai & Iguchi [25] is shown to be the annular under this condition without the expansion.

B For poor wettability ($\theta_c = 147°$)

As mentioned in the introduction, the surface wettability is known to affect the meniscus of the air-water two-phase flow in a narrow channel because the thickness of the present channel, 2 mm, is narrower than the Laplace constant of 2.7 mm. In Fig. 7, the meniscus patterns within two narrow plates are sketched for good ($\theta_c = 30°$) and poor ($\theta_c = 147°$) wettabilities. Therefore, as seen in Fig. 8 (a), case (III) behaves like the annular flow, which is different from case (I) (Kumagai & Iguchi [25] named such a kind of phenomenon the channeling). The vector plots (larger

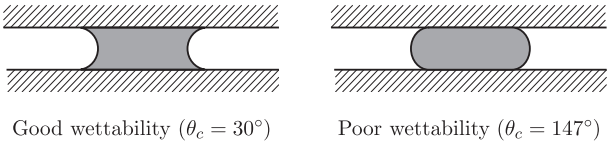

Fig. 7: Meniscus within two narrow plates. The water phase is colored in gray.

velocity plots than 0.4 m/s are erased for facilitating view) and the contour line of the pressure are shown in Fig. 8 (c) and (e). The high airflow rate of case (IV) can produce an intriguing nature that water phase behaves like droplets moving in the air phase due to the large j_g from the nozzle (see Fig. 8 (b)). These droplets grows to slug drops due to merging themselves downstream of about $x = 200$ mm where the pressure drop due to the expansion recovers (see Fig. 4). In addition, the corresponding vector plots (Similar to Fig. 8 (c), larger velocity plots than 0.45 m/s are erased) and the pressure contour are shown in Fig. 8 (d) and (f).

Figure 9 shows the process of the air phase growing to the channeling at the first bubble passing through the expansion. Unlike the result of Fig. 5 about case (I), the air phase cannot be fragmented at the expansion due to the meniscus of the poor wettability (see Fig. 7), and the channeling of the air phase is formed downstream of the expansion.

IV Concluding remarks

This study has implemented the FLUENT computation for gas-liquid two-phase flow in horizontally placed hydrophilic or hydrophobic rectangular channels with an

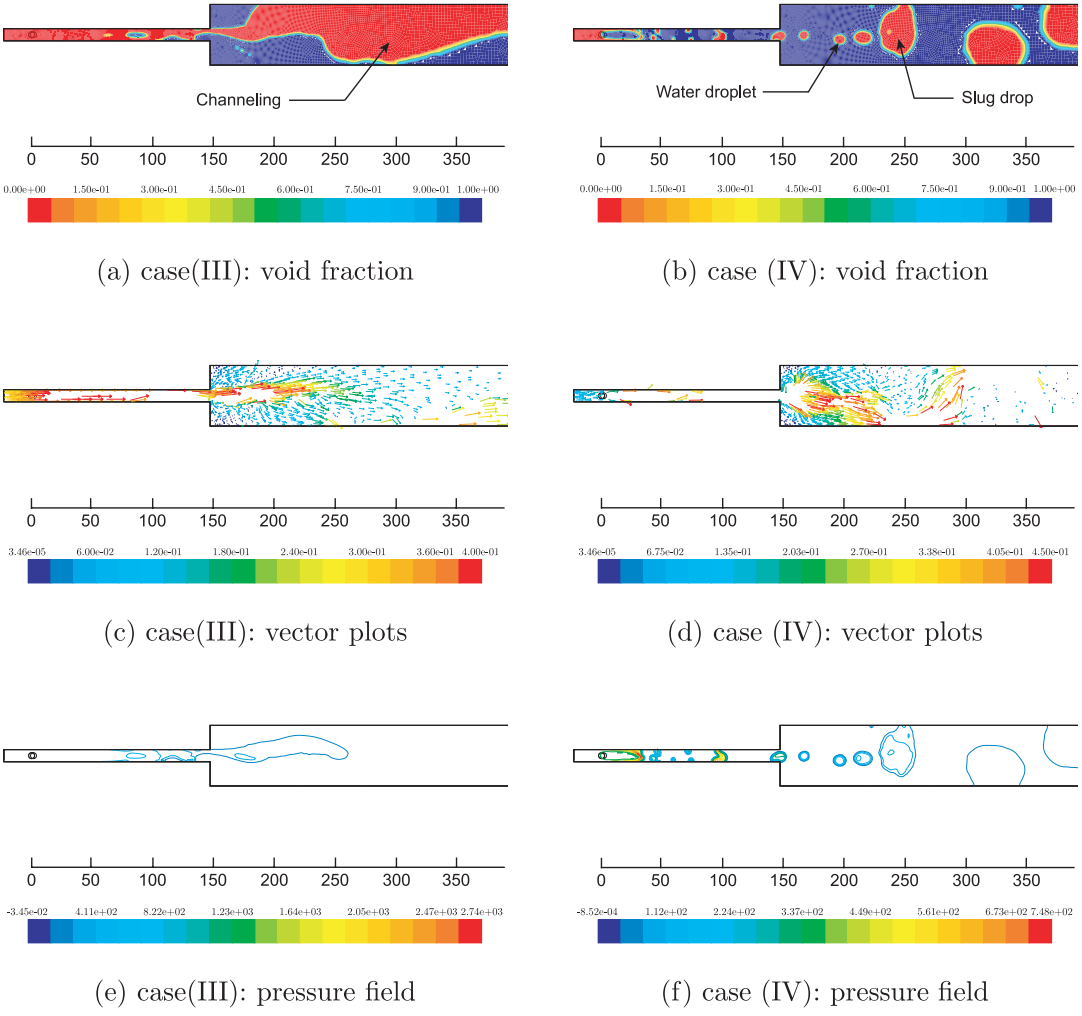

Fig. 8: Flow patterns for cases (III) and (IV). Note that, in the vector plots, larger velocity plots than 0.4 m/s for (c) and 0.45 m/s for (d) are erased for facilitating view.

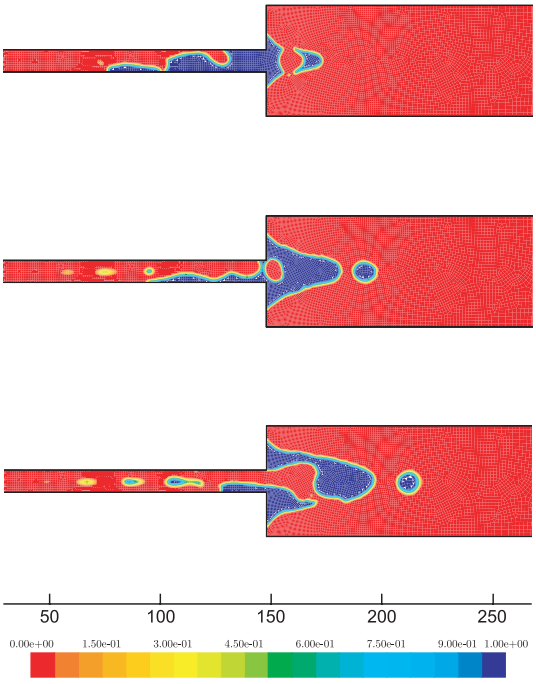

Fig. 9: Selected snapshots of bubble deformation (void fraction) at the expansion for case (III) at (top): $t = 0.4$ s, (middle): $t = 0.5$ s and (bottom): $t = 0.6$ s.

abrupt expansion. These rectangular channels have a thickness narrower than the Laplace constant of this target system. Main findings are as follows:

- Under the good wettability condition, the flow patterns downstream of the expansion were classified into two within the present experimental conditions, i.e., the bubble fragments pattern for the low j_g (case (I)) and the annular-like flow pattern for the high j_g (case (II)). These computed flow patterns were in nice agreement with the previous experimental results [23].
- The fragments of the bubble in case (I) grows to slug bubbles in downstream due to pressure recovery of the channel flow.
- Under the poor wettability condition, the meniscus affects the flow pattern because of the narrower thickness of the channel than the Laplace constant. In the low j_g (case (III)), the water phase forms the channeling whereas the water phase behaves like droplets moving in the air phase (case (IV)).

Unfortunately, there is no experimental data under a poor wettability condition about these kinds of rectangular ducts with an abrupt expansion. To properly verify the present computational results of cases (III) and (IV), the experiment needs to be carried out.

Received: March 16, 2012. Accepted: July 10, 2012.

References

[1] G.I. Taylor, *J. Fluid Mech.*, **10**, 161–165 (1961).
[2] R.M. Davies and G.I. Taylor, *Proc. R. Soc. Lond.*, A**200**, 375–390 (1950).
[3] G.F. Hewitt and D.N. Roberts, *United Kingdom Atomic Energy Authority (UKAEA) Report*, AERE-M2159 (1969).
[4] O. Baker, *Oil and Gas J.*, **53**, 185–190 (1954).
[5] Y. Taitel and A.E. Dukler, *AIChE J.*, **22**, 47–55 (1976).
[6] S. Waelchli, P. Rudolf and R. von Rohr, *Int. J. Multiphase Flow*, **32**, 791–806 (2006).
[7] K.A. Triplett, S.M. Ghiaasiaan, S.I. Abdel-Khalik and D.L. Sadowski, *Int. J. Multiphase Flow*, **25**, 377–394 (1999).
[8] U. Kadri, M.L. Zoeteweij, R.F. Mudde and R.V.A. Oliemans, *Int. J. Multiphase Flow*, **35**, 439–449 (2009).
[9] M. Dziubinski, H. Fidos and M. Sosno, *Int. J. Multiphase Flow*, **30**, 551–563 (2004).
[10] The Japan Society of Mechanical Engineers, *Handbook of gas-liquid two-phase flow technology*, Corona press, (2006).
[11] M. Iguchi and O.J. Ilegbusi, *Modeling multiphase materials processes*, Springer, (2010).
[12] R.W. Lockhart and R.C. Martinelli, *Chem. Eng. Prog.*, **5**, 39–48 (1949).
[13] D. Chisholm, *Int. J. Heat Mass Transfer*, **10**, 1767–1778 (1967).
[14] J.L. Xu, P. Cheng and T.S. Zhao, *Int. J. Multiphase Flow*, **25**, 411–432 (1999).
[15] H.J. Lee and S.Y. Lee, *Int. J. Multiphase Flow*, **27**, 783–796 (2001).
[16] H.J. Lee and S.Y. Lee, *Int. J. Multiphase Flow*, **27**, 2043–2062 (2001).
[17] M. Sadatomi, M.I. Ali and M. Kawaji, *Trans. JSME*, (B) **58**-546, 408–415 (1992).
[18] T. Sawai, M. Kaji and G. Matsui, *Trans. JSME*, (B) **71**-710, 2427–2433 (2005).
[19] F. Aloui and M. Souhar, *Int. J. Multiphase Flow*, **22**, 849–861 (1996).
[20] I.M. Ali, M. Sadatomi and M. Kawaji, *Can. J. Chem. Eng.*, **71**, 657–666 (1993).
[21] M. Iguchi and Y. Terauchi, *Int. J. Multiphase Flow*, **27**, 729–735 (2001).
[22] K. Fukushi and M. Iguchi, *J. JSEM*, **4**, 192–197 (2004).
[23] T. Oke, T. Kumagai and M. Iguchi, *J. JSEM*, **10**, 32–37 (2010).
[24] FLUENT 6.2 User's Guide, Fluent Inc., Lebanon, NH (2005).
[25] T. Kumagai and M. Iguchi, *J. JSEM*, **7**, 50–55 (2007).
[26] W.H. Ahmed, C.Y. Ching and M. Shoukri, *Int. J. Multiphase Flow*, **33**, 575–594 (2007).